Cardiovasc Intervent Radiol (2020) 43:311–321
https://doi.org/10.1007/s00270-019-02343-1

Hepatic Arterial Bland Embolization Increases Th17 Cell Infiltration in a Syngeneic Rat Model of Hepatocellular Carcinoma

Rony Avritscher[1] · NaHyun Jo[1] · Urszula Polak[1] · Andrea C. Cortes[1] · Hideyuki Nishiofuku[2] · Bruno C. Odisio[1] · Haruyuki Takaki[3] · Alda L. Tam[1] · Marites P. Melancon[1] · Steven Yevich[1] · Aliya Qayyum[4] · Ahmed Kaseb[5] · Kimihiko Kichikawa[2] · Sanjay Gupta[1] · S. Nahum Goldberg[6,7] · Seon Hee Chang[8]

Received: 14 April 2019 / Revised: 20 August 2019 / Accepted: 17 September 2019 / Published online: 7 October 2019

Abstract

Purpose To determine the tumor immune cell landscape after transcatheter arterial bland embolization (TAE) in a clinically relevant rat hepatocellular carcinoma (HCC) model.

Materials and Methods Buffalo rats ($n = 21$) bearing syngeneic McArdle RH-7777 rat hepatoma cells implanted into the left hepatic lobe underwent TAE using 70–150 μm beads ($n = 9$) or hepatic artery saline infusion ($n = 12$). HCC nodules, peritumoral margin, adjacent non-cancerous liver, and splenic parenchyma were collected and disaggregated to generate single-cell suspensions for immunological characterization 14 d after treatment. Changes in tumor-infiltrating immune subsets including CD4 T cells (Th17 and Treg), CD8 cytotoxic T cells (IFNγ), and neutrophils were evaluated by multiparameter flow cytometry. Migration and colony formation assays were performed to examine the effect of IL-17, a signature cytokine of Th17 cells, on McArdle RH-7777 hepatoma cells under conditions simulating post-embolization environment (i.e., hypoxia and nutrient privation). Statistical significance was determined by the Student unpaired t test or one-way ANOVA.

Results TAE induces increased infiltration of Th17 cells in liver tumors when compared with controls 14 d after treatment (0.29 ± 0.01 vs. 0.19 ± 0.02; $p = 0.02$). A similar pattern was observed in the spleen (1.41 ± 0.13 vs. 0.57 ± 0.08; $p < 0.001$), indicating both local and systemic effect. No significant differences in the percentage of FoxP3 + Tregs, IFNγ-producing CD4 T cells, and CD8 T cells were observed between groups ($p > 0.05$). In vitro post-embolization assays demonstrated that IL-17 reduces McA-RH7777 cell migration at 24–48 h ($p = 0.003$ and $p = 0.002$, respectively).

Conclusion Transcatheter hepatic arterial bland embolization induces local and systemic increased

Electronic supplementary material The online version of this article (https://doi.org/10.1007/s00270-019-02343-1) contains supplementary material, which is available to authorized users.

✉ Rony Avritscher
rony.avritscher@mdanderson.org

[1] Department of Interventional Radiology, The University of Texas MD Anderson Cancer Center, 1515 Holcombe Blvd, Houston, TX 77030, USA

[2] Department of Radiology, IVR Center, Nara Medical University, 840 Shijo-cho, Kashihara 634-8522, Japan

[3] Department of Radiological Technology, Hyogo College of Medicine College Hospital, 1-1 Mukogawa-cho, Nishinomiya 663-8501, Hyogo, Japan

[4] Department of Diagnostic Radiology, The University of Texas MD Anderson Cancer Center, Houston, TX 77030, USA

[5] Department of Gastrointestinal Medical Oncology, The University of Texas MD Anderson Cancer Center, Houston, TX 77030, USA

[6] Laboratory for Minimally Invasive Tumor Therapies, Department of Radiology, Beth Israel Deaconess Medical Center, Harvard Medical School, Boston, MA 02215, USA

[7] Department of Radiology, Hadassah Hebrew University Medical Center, Jerusalem, Israel

[8] Department of Immunology, The University of Texas MD Anderson Cancer Center, Houston, TX 77054, USA

infiltration of Th17 cells and expression of their signature cytokine IL-17. In a simulated post-embolization environment, IL-17 significantly reduced McA-RH7777 cell migration.

Keywords Th17 cells · IL-17 · Transcatheter hepatic arterial bland embolization · Tumor-infiltrating lymphocytes · HCC immune landscape

Introduction

Transcatheter hepatic arterial bland embolization (TAE), conventional transarterial chemoembolization (cTACE), and TACE with drug-eluting beads (DEB-TACE) remain the mainstays of catheter-based locoregional treatment for intermediate (stage B) and advanced-stage (stage C) hepatocellular carcinoma (HCC) patients, according to the Barcelona Clinic Liver Cancer (BCLC) staging system [1–3]. These approaches offer survival benefit for selected patients, but recurrence rates remain high [4]. Critical to the effectiveness of both TAE and cTACE/DEB-TACE is tumor hypoxia and resulting tissue necrosis secondary to acute vascular occlusion. This acute necrotic cell death is widely recognized as a potent activator of adaptive immunity [5]. Indeed, several investigators have reported various alterations in circulating T cell profiles after cTACE and TAE alone [6–8].

Because the interplay between a cancer cell and its surroundings plays a central role in antitumor immune responses, it is essential to determine, not only circulating T cell profiles, but also the impact of these therapies on the local tumor immune microenvironment. Cancer treatment often leads to immunosuppressive environments and can represent an obstacle for effective T cell responses [9–11]. In these suppressive environments, T cell activation is downregulated through signaling exerted by different members of the CD28 receptor family, such as cytotoxic T-lymphocyte antigen 4 (CTLA-4), programmed death-1 (PD-1), B and T lymphocyte attenuator (BTLA), and T cell immunoreceptor with Ig and tyrosine-based inhibition domains (TIGIT) [12–15]. Additional co-inhibitory receptors such as T cell immunoglobulin and mucin domain-containing protein 3 (Tim-3), lymphocyte activation gene-3 (LAG-3), and Tregs also shift the balance of effective antitumor T cell response to a more tolerogenic or immunosuppressive tumor microenvironment [16–18].

Thus, measuring circulating cells and cytokines after treatment is not sufficient to unravel the complexities involved in the attraction and survival of T cells in tumor stroma. Rather, a more detailed characterization of the various subsets of tumor-infiltrating lymphocyte populations beyond general T cell population description and CD4 + /CD8 + ratios is needed for successful development of combined therapies.

In this study, we aimed to characterize tumor immune cell landscape after transcatheter arterial bland embolization, including key T cell subsets, in a clinically relevant syngeneic immunocompetent rat hepatoma model and the effect of their signature cytokine(s) upon tumor cells in the context of post-embolization environment. We have chosen TAE as a starting point to investigate the effects of transcatheter arterial embolization on the tumor immune microenvironment to better characterize the nature of infiltrating immune cell populations secondary to acute tumor ischemia without the confounding presence of concurrent chemotherapeutic agents.

Materials and Methods

Study Design and Animal Model

Experimental procedures were approved by our institutional animal care and use committee and were performed in accordance with institutional guidelines. Male Buffalo rats (Charles River Laboratories, Wilmington, MA), with a weight range of 0.27 to 0.35 kg, were used in these experiments. Animals were allowed free access to rat chow and water and housed under a standard light–dark schedule (12-hour phase shift). After anesthesia (2–3% isoflurane/2 L/min oxygen), a midline mini-laparotomy was performed to expose the liver. A total of 100 µL of 1×10^6 McA-RH7777 (CRL-1601, ATCC, Manassas, VA, USA) rat hepatocellular carcinoma cells in 2% normal rat serum-saline solution was slowly injected into the subcapsular portion of the left hepatic lobe, according to the Morris HCC model in Buffalo rats, as previously published in the literature [19]. Abdominal incision was closed with a two-layer technique. Tumor nodules were allowed to grow for 3 weeks (Fig. 2A). Subsequently, rats were randomly divided into two groups (bland embolization and sham-saline injection) and evaluated 14 days after image-guided procedure. This time point was selected based on previous reports showing a T cells peak response in peripheral blood 14 d after locoregional therapies [8, 20].

This study was performed in two separate phases (Fig. 1). In the first phase, we quantified relevant immune cell populations and their signature cytokines in the tumor, peritumoral region, non-cancerous surrounding liver, and spleen using multiparameter flow cytometry to characterize local and systemic patterns of tumor-infiltrating lymphocytes after bland embolization. Splenic tissue was analyzed

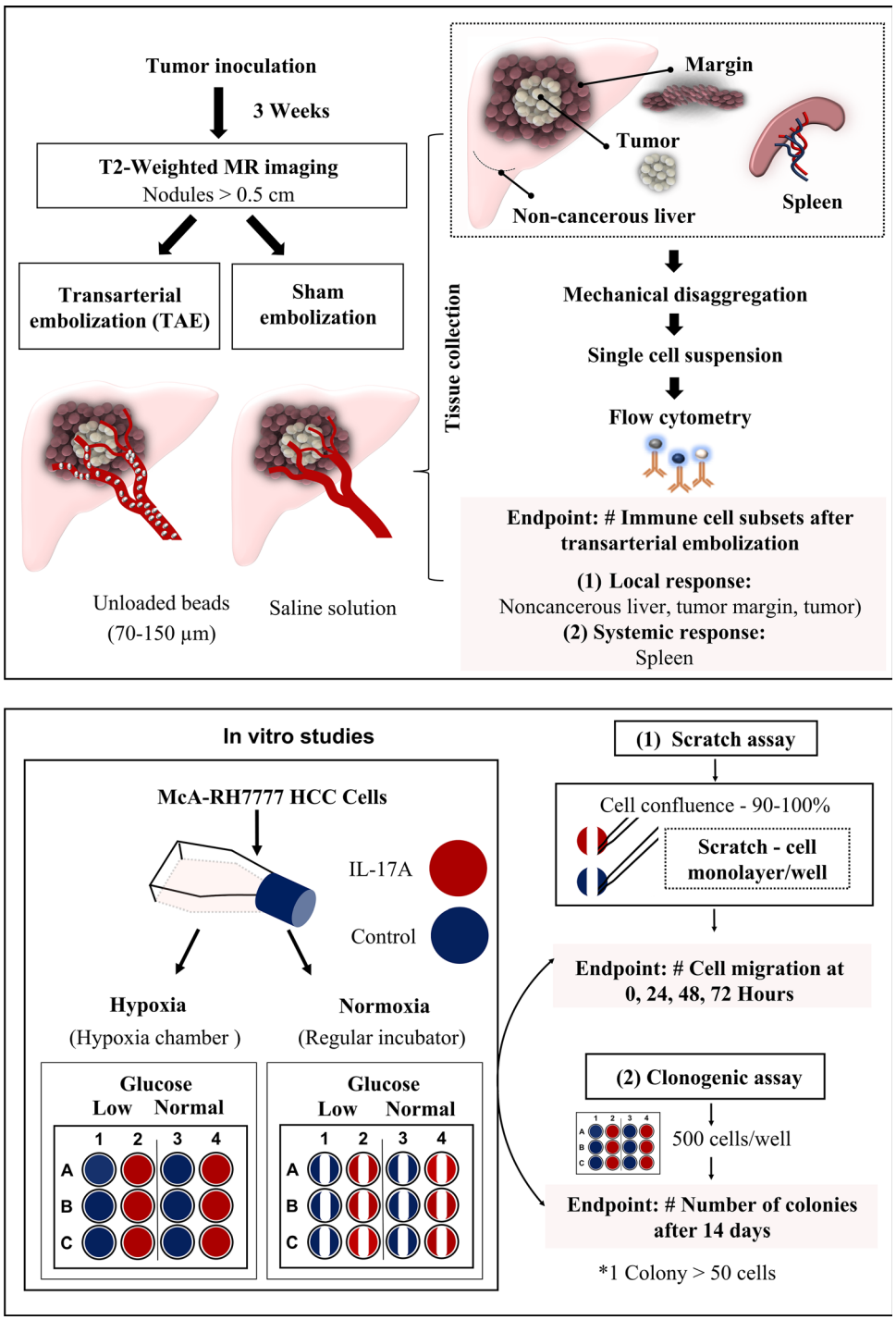

Fig. 1 Schematic diagram of the workflow sequence for in vivo experiments designed to assess systemic and local differences in immune cell subsets after transarterial bland embolization (upper panel). Experimental design of the in vitro studies aimed to mimic environmental features of embolization to evaluate cell migration and colony formation ability of McA-RH7777 cells in response to the exogenous addition of IL-17A (bottom panel)

to determine whether local tumor embolization had any effects upon extrahepatic populations of T cells. Next, given the fact that the precise effects of signature cytokine(s) on tumor cells vary widely from antitumor to tumorigenic depending on the context of the tissue microenvironment, we conducted a second phase where McA-RH7777 cells were treated with relevant cytokine(s) identified during the first phase in the specific context of post-embolization conditions. The relevant cytokine(s) were subsequently added to these cell cultures and their effect on cell colony formation and migratory potential was recorded to elucidate their pro- or anti-tumorigenic potential.

Image-Guided Intra-Arterial Therapy

T2-weighted MR imaging was performed on anesthetized animals the day before treatment using a 4.7 T MR scanner (Biospec, Bruker Biospin MRI) to confirm the size and location of the tumor nodules using imaging protocols previously described [21]. Subsequently, anesthetized rats with minimum tumor diameters of 0.5 cm, underwent hepatic arterial catheterization using a common carotid artery (CCA) approach as previously described [22]. Briefly, left CCA was cannulated by a 20-gauge intravenous catheter (Angiocath—IV catheter; 20GX1.16″) under a dissecting microscope. Endovascular instrumentation was conducted using 1.6-Fr microcatheter (Tokai medical, Japan) and, a 0.014-inch guidewire (Transcend; Boston Scientific). Manual injection of iodixanol injectable contrast medium (Visipaque; GE Healthcare) was delivered through the catheter, as needed, to visualize the hepatic vasculature [22]. Embolic agent, 70–150 µm beads (DC Bead, BTG, Surrey, UK) [23], was resuspended in saline solution and mixed with contrast medium (1:1 ratio). A total volume of 1 mL from the mixture with or without beads (sham controls) was delivered into the proper hepatic artery under fluoroscopic guidance. The endpoint of the embolization was the delivery of the complete dose of 1 mL of the mixture or until near stasis of blood flow (Fig. 2B, C). After the intervention, intra-arterial catheter was removed, and left CCA ligated. The two-layer technique was used to close the neck incision.

Tissue Collection and Isolation of Immune Cells from Liver and Spleen

Two weeks after the procedure, isoflurane-anesthetized rats were euthanized, and the spleen and liver tumors were harvested from rats previously treated with TAE (n = 9) or saline infusion only (n = 12). Freshly collected specimens were promptly transferred to phosphate-buffered saline (PBS) plus 2% heat-inactivated fetal bovine serum (FBS; Sigma-Aldrich, St. Louis MO) for flow cytometric analyses. Representative specimens from each group were preserved in 10% neutral-buffered formalin and stained with hematoxylin and eosin stains (H&E). Liver sections in 2% FBS-PBS were further divided into tumor, peritumoral margin, and adjacent non-cancerous liver (> 1 cm of distance from the tumor nodule) according to the standardized guidelines for the assessment of tumor-infiltrating lymphocytes in solid tumors [24]. Tissue sections in 2% FBS-PBS were weighed and processed into single-cell suspensions by mechanical dissociation through a 70-µM nylon mesh.

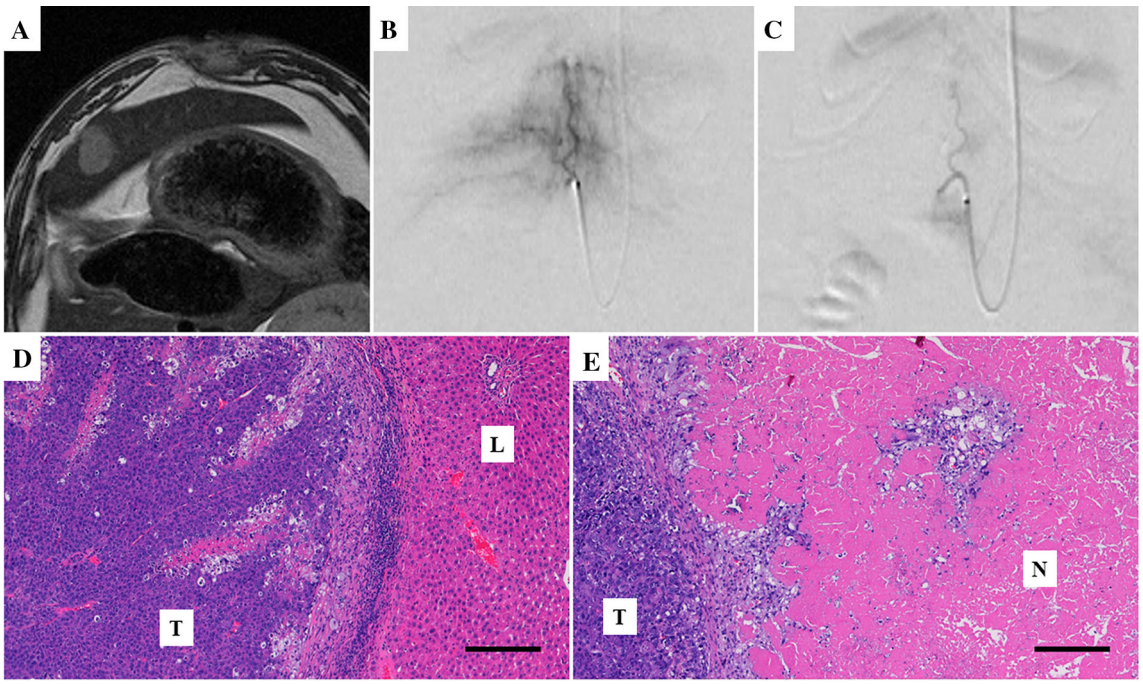

Fig. 2 Hepatoma nodule progression in the Buffalo rat orthotopic model. **A** T2-weighted MR image of solitary liver tumor obtained in a Bruker 4.7 T magnet. **B–C** Digital subtraction angiography (DSA) images before and after embolization of left liver tumor with a fixed dose of 4000 unloaded beads (70–150 µm; DC Bead, BTG, Surrey, UK) suspended in a mixture of a contrast medium and saline solution (1 mL). **D–E** H&E-stained tissue sections show viable tumor (T) and adjacent unaffected liver (L) in control animal and exuberant tumor tissue necrosis (N) after embolization in post-treatment animal. Scale bar: 200 microns. Original magnification 10X

Immune Phenotyping

Cells suspensions were centrifuged at 1500 rpm for 5 min at 4 °C. Subsequently, cell pellets were resuspended in 40% Percoll-PBS solution (GE Healthcare, USA) followed by centrifugation at 4500 rpm for 20 min at 4 °C. After centrifugation, pellets of immune cells were collected and washed twice with PBS at 1500 rpm for 5 min at 4 °C. Mononuclear cells, normalized to tissue weight, were stained for surface antigens at 4 °C for 20 min in the presence of FcBlock to detect: CD4 T cells, CD8 T cells, RP-1 positive cells (neutrophils), and CD11b/c positive cells (include monocytes, macrophages, and dendritic cells). Antibodies used for immunophenotyping are described in Table 1. For the detection of intracellular markers (IL-17A, IFN-γ, and Foxp3), immune cells were restimulated with PMA (20 ng/ml) plus Ionomycin (1 μg/ml) in the presence of a protein transport inhibitor, Brefeldin A, for 5 h. After surface staining, cells were fixed and permeabilized using eBioscience Foxp3/Transcription Factor Staining Buffer Set or BD Cytofix/Cytoperm Fixation/Permeabilization Solution Kit for IL-17A, IFN-γ. Cells were stained for intracellular cytokines and FOXP3 transcription factor at 4 °C for 20 min. Finally, cells were analyzed on a LSRII flow cytometer (Beckman Coulter), and data were further analyzed using FlowJo (Tree Star Inc). Our gating strategy is presented in Fig. S1.

In Vitro Studies

Given that tumor embolization typically leads to two major defining environmental features, nutrient restriction and hypoxia [25–27] and that our in vivo experiments identified Th17 cells (recognized by IL-17 production) as important immune cell subtype after TAE, the second phase of our study aimed to evaluate differences in the migratory potential and colony formation of McA-RH7777 cells induced by the exogenous addition of IL-17A. Consequently, McA-RH7777 cells were cultured under hypoxia and glucose restriction to mimic the context of bland embolization microenvironment in vitro (Fig. 1).

Cell Line and Reagents

McA-RH7777 rat hepatoma cell line, derived from the Buffalo rat, was maintained in corning Dulbecco's modified Eagle's Medium (DMEM) with L-glutamine, 4.5 g/L glucose, and sodium pyruvate (Corning), supplemented with 10% FBS in a humidified atmosphere at 37 °C, 5% CO2. Nutrient-deprived conditions were performed using DMEM-Low glucose (1000 mg/L glucose) with L-glutamate and sodium bicarbonate (Millipore Sigma, St. Louis, MO). Rat recombinant Interleukin-17A (IL-17A) was purchased from ProSpec-Tany TechnoGene, Rehovot, Israel (#CYT-542).

Cell Migration Assay

Cell migration potential was observed by using the in vitro scratch assay, in which a cell-free area is created by mechanical scratching a confluent cell monolayer and, subsequently, capturing the images of the scratch at regular intervals and comparing scratch widths to quantify variations in the relative wound area due to cell migration [28]. To this end, McA-RH7777 cells (5×10^5 cells/well) were plated in flat bottom 96-well plates and incubated at 90% confluency. Following serum starvation (0.5% FBS-DMEM) for 16 h to synchronize the cell cycle, the scratch was made in the confluent monolayer using a pipette tip to leave a scratch of approximately 0.4–0.5 mm in width. After the scratch wound was made, cells were cultured in DMEM-low glucose or normal glucose (4.5 g/L) with or without 50 ng/mL of IL-17A. Cell media was supplemented with 2% FBS to inhibit cell proliferation during the duration of the assay. Plates were incubated in a 37 °C regular incubator (20% oxygen) or in a hypoxia incubator chamber (5% oxygen, STEMCELL Technologies) to investigate the effect of IL-17A under a normoxic or hypoxic environment. Serial pictures, after the scratch

Table 1 List of antibodies used in flow cytometry

Antibody	Fluorochrome	Clone	Manufacturer	Catalog number
Anti-Rat CD32 (FcγII receptor)	(FcBlock)	D34-485	BD Bioscience	#550270
Anti-Rat Granulocytes	PE	RP1	BD Bioscience	#550002
Anti-Rat CD3	FITC	1F4	BD Bioscience	#561801
Anti-Rat CD11b/c	PerCP/Cy5.5	OX-42	Biolegend	#201819
Anti-Rat CD4	APC/Cy7	W3/25	Biolegend	#201517
Anti-Rat CD8a	V450	OX-8	BD Bioscience	#561614
Anti-Rat IFN-γ	Alexa Fluor 647	DB-1	BD Bioscience	#562213
Anti-Mouse/Rat IL-17	PE	eBio17B7	eBioscience	#12-7177-81
Anti-Mouse/Rat Foxp3	APC	FJK-16s	eBioscience	#77-5775-40

wound was made, were taken at 0, 24, 48, and 72 h under a microscope. Changes in the relative wound area were measured in pixels using MRI Wound Healing Tool-ImageJ [29]. To minimize sampling error, experiments were performed in triplicate and repeated three times. Data presented as the percentage by which the original scratch width decreased for each consecutive time point.

Clonogenic Assay

McA-RH7777 cells were seeded at 5×10^2 cells per well in six-well plates. Cells were cultured during 12 d in normal- or low-glucose medium, with or without 50 ng/mL of IL-17A. Plates were incubated under normoxia or within the hypoxic chamber as described above. After 12 d, cells were fixed (100% methanol) and stained with 0.5% Crystal violet (in 25% methanol) [30]. Only colonies with > 50 cells were manually counted [31]. Experiments were performed in triplicate and repeated twice.

Statistical Evaluation

Statistical analysis was performed using GraphPad Prism (version 7). Data represent the mean ± standard error of the mean. Statistical significance was determined by the Student unpaired t test or one-way ANOVA with Tukey's multiple comparisons test. $p < 0.05$ was considered to represent a significant difference. The resource equation approach was used to calculate the minimum number of animals required per group [32].

Results

Hepatic Arterial Bland Embolization Induces Increased Infiltration of Th17 Cells in Liver and HCC Tumor Nodules

In keeping with prior studies, approximately 60–70% of the tumor and adjacent non-cancerous liver immune cells (20% T cells and 40–50% of RP-1 cells) and 40% of total spleen cell types (30% of T cells and 10% of RP-1 cells) were successfully analyzed by immunophenotyping [33]. Of all subtypes studied, quantitative multiparameter analysis showed that only the percentage of IL-17 + CD4 T cells (Th17) cells in liver tumors was significantly higher in animals treated with bland embolization compared with the control group at 14 d (0.29 ± 0.01 vs. 0.19 ± 0.02; $p = 0.02$), while Th17 cells in tumor margin area remained similar between the two groups. Comparable results were observed in adjacent non-cancerous liver (4.76 ± 0.49 vs. 1.95 ± 0.18; $p < 0.001$) (Fig. 3A). Increase in Th17 cells after bland embolization was of a systemic nature, since we also observed a similar pattern in the spleen after 14 d of TAE (1.41 ± 0.13 vs. 0.57 ± 0.08; $p < 0.001$) (Fig. 3B). Th17 cells made up of 60% of IL-17-producing cells in the liver, while approximately 20% of IL-17 was produced by CD8 T cells. IL-17-producing cells were also detected in the CD4 T cell fraction of spleen, in a similar fashion (Fig. 3C).

IL-17 Inhibits in Vitro McA-RH7777 Hepatoma Cells Cell Migration in Low-Nutritional, Hypoxic Environment, But Does Not Affect Cell Proliferation

McA-RH7777 cells treated with IL-17 and cultured in a low-nutritional environment demonstrated decreased migratory potential. Results showed a statistically significant difference in the relative percentage of open scratch area at 24 h (19.47 ± 0.98 vs. 23.69 ± 2.52; $p = 0.003$) and 48 h (7.13 ± 3.28 vs. 15.34 ± 3.50: $p = 0.002$) from initial scratch (Fig. 4A, B, S Table 1). Colony formation assay showed higher proliferation potential of McA-RH7777 cells in low-glucose media compared to regular-glucose media under both normoxic (183.3 ± 36.58 vs. 142.7 ± 31.56; $p = 0.004$) and hypoxic conditions (275.6 ± 33.91 vs. 217.3 ± 27.26, $p = 0.02$). However, no significant difference found with and without IL-17 treatment in both nutritional environments and different oxygen concentrations (Fig. 5A, B, S Table 2).

Treg, cytotoxic CD8 T cell, and neutrophil infiltration was not affected by hepatic arterial embolization

Total number of infiltrating mononuclear cells in the tumor, margin, and adjacent non-cancerous liver were similar and did not change significantly upon embolization ($1.9 \pm 1.0 \times 10^6$ cells/g of adjacent non-cancerous liver tissue versus $2.3 \pm 0.8 \times 10^6$ cells/g of tumor tissue). Foxp3-positive cells among CD4 T cells (Tregs) and IFNγ CD8 T cells were similar between non-treated and embolization treated groups. RP-1 (rat neutrophils marker) positive cells remained similar after TAE (Fig. S2).

Discussion

Combination of locoregional liver treatments with active immunotherapy is regarded as a promising strategy for patients with unresectable liver cancer. Ischemic tumor necrosis caused by transcatheter hepatic arterial bland embolization (and one of the primary cytotoxic effects of TACE) leads to enhanced exposure of tumor antigens to a host of professional antigen-presenting cells, which can activate T cell immunity directed at the tumor. Flow

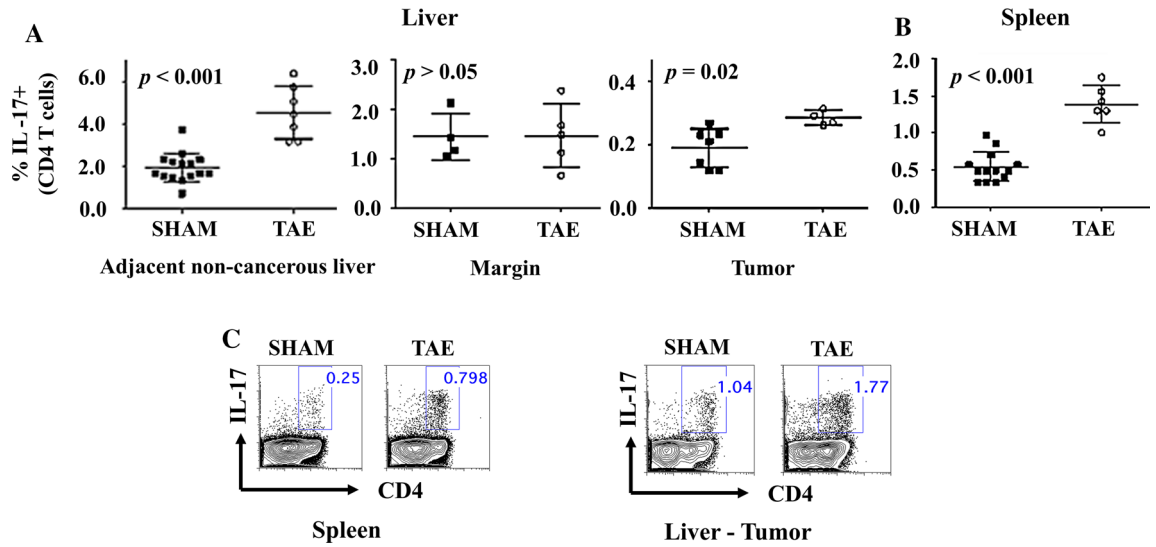

Fig. 3 Increased frequency of Th17 cells in lymphoid organs and tumor-bearing liver after embolization. **A** Significant differences in the frequency of IL-17 producing in response to bland embolization (TAE) in non-cancerous surrounding liver and tumor microenvironment. **B** Higher frequency of IL-17 producing in the spleen after 14 d of TAE. Graph represents pooled data from three or four biologically independent experiments. **C** Representative contour plots of IL-17 expression in CD4 cells in spleen and liver tumor

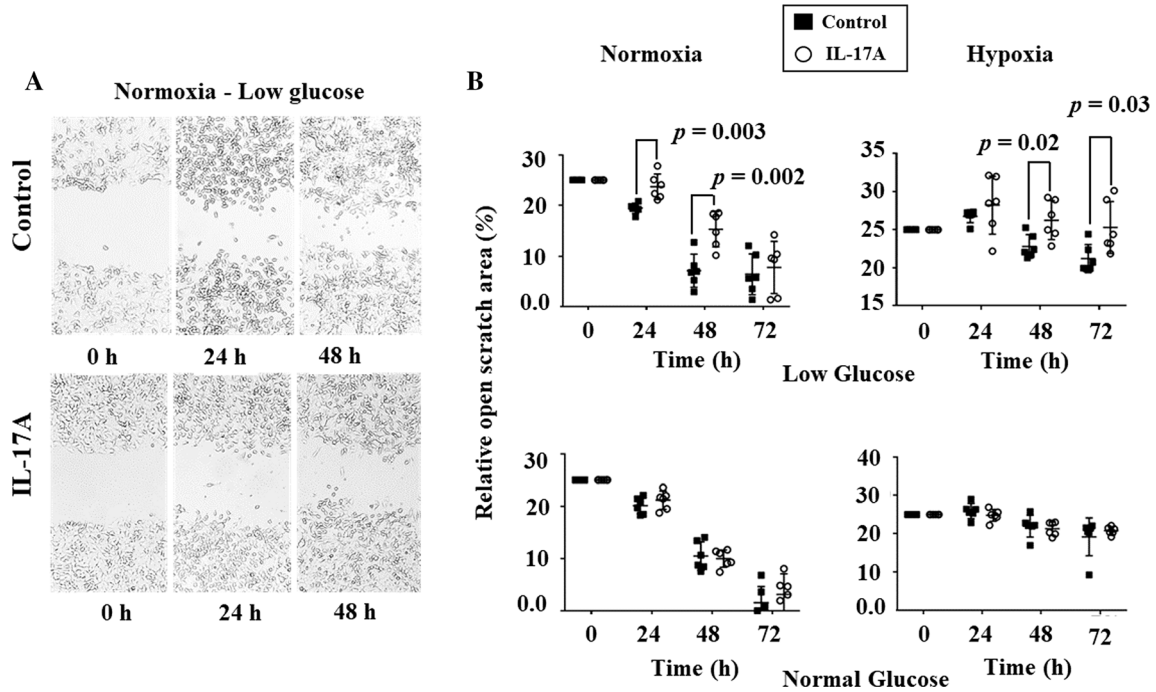

Fig. 4 IL-17A inhibits migration of McA-RH7777 cells in glucose restriction. **A** Representative images of McA-RH7777 cell migration across linear scratch wounds at different time points. (b) Relative percentage of scratch open area after 0, 24, 48, and 72 h of treatment with and without IL-17A. Scratch open area was measured in the control and IL-17A treated cells exposed to normal or glucose restriction media under normoxia (∼ 20% oxygen) or hypoxia (5% oxygen) cell culture conditions. Results of three independent experiments are presented

cytometry data provided a characterization of the tumor adaptive immune microenvironment landscape after TAE, and this deeper understanding is essential for the development of novel combination strategies. Our study demonstrates that only one specialized subset of T helper lymphocytes, Th17 cells, and its signature cytokine IL-17, are consistently increased in the tumor microenvironment after TAE.

Liver cancer immune cell landscape after catheter-directed therapy has not been characterized. Studies dealing

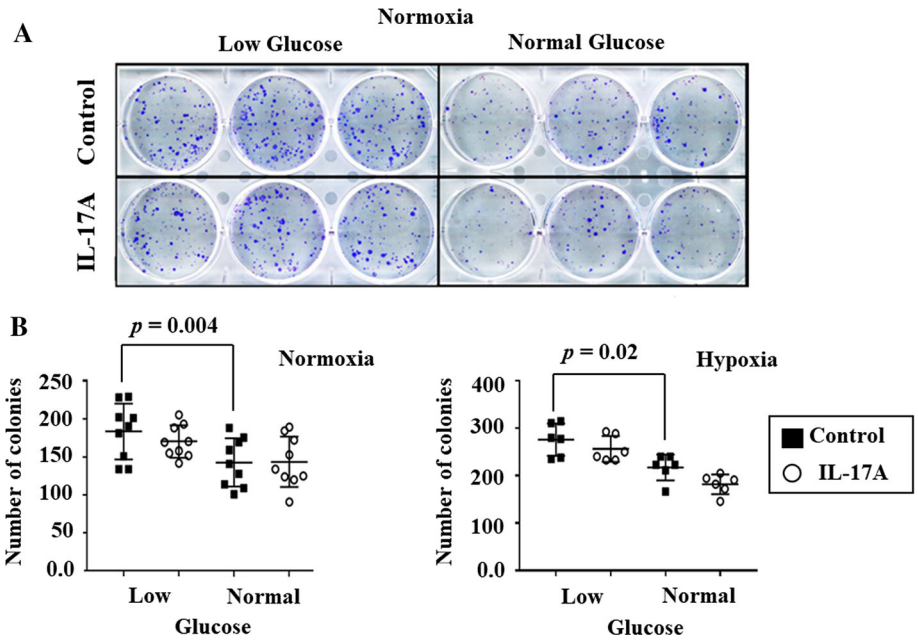

Fig. 5 Glucose restriction increases colony formation ability of McA-RH7777 cells under different oxygen levels. **A** Representative images of colonies formed from McA-RH7777 cells treated with 50 ng/mL of IL-17A under normal or glucose restriction in a normoxic environment (~ 20% oxygen). **B** Significant differences between the number of colonies formed after 12 d of cell culture under glucose restriction in normoxia and hypoxia. IL-17A treatment exerted no significant effect over McA-RH7777 colony formation ability in any of the cell growth conditions tested. Crystal violet staining was performed to evaluate the number of colonies under a stereomicroscope. Results of three independent experiments are presented

with the impact of hepatic arterial embolization on the immune system have mostly focused on circulating peripheral cells in HCC patients. Liao et al. [34] conducted a thorough analysis of circulating immune cells subsets including CD4 + cells (Th1, Th17, and Treg cells), CD8 + T cells, NK cells, and NKT cells, as well as plasma cytokines before and after TACE, where they only observed a significant increase in the frequency of circulating Th17 cells after TACE, when compared to baseline. A separate study also quantifying circulating cytokines after TACE showed significantly higher levels of IL-17 after treatment [35]. More recently, while reporting on systemic immune response after microwave ablation, Zhou et al. [36] observed that of all relevant circulating T cell subsets, only the frequency of Th17 cells was significantly increased after treatment with unchanged levels of CD3 + , CD4 + , CD8 + , and Tregs. Our findings in the local immune microenvironment reflect these systemic alterations.

Interleukin-17 (IL-17) expression is the hallmark of Th17 cells. IL-17 is responsible for neutrophil recruitment with well-established roles in autoimmunity disorders and infections, but its effect in tumors remains controversial. It has been hypothesized that IL-17 can play a dual role in cancer with pro-tumor or antitumor effects [37, 38]. In a seminal article by Benchetrit, IL-17 was shown to inhibit tumor cell growth by T cell-dependent mechanism in immunocompetent hosts [39]. IL-17 can also promote tumor growth via IL-6-mediated activation of STAT3 in cancer cells resulting in increased transcription of proliferation and angiogenic genes [40, 41]. This pathway has been also described as clinically relevant for image-guided ablative techniques by several authors [42, 43]. Gu et al. also demonstrated that IL-17 can augment secretion of proinvasive factors and promote angiogenesis, neutrophil recruitment and tumor growth [44]. Therefore, IL-17 appears to be a pleiotropic cytokine, and the direct effects of IL-17 depend on the context of the tumor microenvironment.

To assess IL-17 effects on McA-RH7777 cells in a post-embolization environment, we designed assays subjecting tumor cells to hypoxia and low nutrient conditions. IL-17 reduced tumor cell migration suggesting that, in the context of TAE, Th17 cells and IL-17 may play an antitumor role. These results are consistent with previously published circulating Th17 data showing that increased frequency of those cells in circulation after 30 days correlated with improved patient survival [34]. In a separate study, intratumoral IL-17 in non-embolized hepatocellular carcinoma was associated with poorer patient survival and increased recurrence [45]. These findings help illustrate the dual role of IL-17 in the tumor immune microenvironment, based on the nature of the peritumoral inflammatory milieu.

Our results demonstrated that the necrotic cell death after bland embolization did not have a significant effect upon migration of CD8 T cells or Tregs. These results are consistent with a recent study by Yarchoan et al. [46] in which it was determined that the mean density of CD8 T cells was higher on the normal liver than in the actual tumor. In another study, Duan et al. reported that CD8 T cells surrounding residual tumors were markedly increased in the radiofrequency ablation (RFA) only and RFA plus TAE groups on day 7. However, the group undergoing TAE alone showed a less pronounced effect on CD8 T cell infiltration, in line with our results and other previous characterizations of the HCC immune environment. These findings suggest that the combination of modalities may have a synergistic effect [8]. In addition, due to the immunogenic nature of cell death caused by anthracyclines, it is also conceivable that transcatheter hepatic arterial chemoembolization with doxorubicin may result in stronger CD8 T cell infiltration [47].

This study represents a first exploratory report addressing the complexity of cellular immune response in HCC tumor microenvironment in a syngeneic tumor model in immunocompetent animals after bland transarterial embolization. However, it is important to acknowledge relevant limitations. Although a much greater variety of antibody reagents exists for mouse models, limited reagents were available for rat immune cells. Nevertheless, we by necessity used a rat model to better emulate human endovascular interventions and the biological effects of transcatheter embolization, due to diminutive murine vasculature and the inherent inability to routinely cannulate and navigate mouse hepatic vessels. TAE is one of the many therapeutic approaches for locoregional treatment of HCC and chemoembolization remains the mainstay of catheter-based therapies. While animals included in our study did not exhibit clinical signs of distress throughout the course of our experiments, and thereafter, dedicated imaging assessment of potential post-procedural complications that could have compounded the immune response to TAE was not performed. In our study, we only analyzed the cellular changes after TAE and the added effect of cytotoxic chemotherapy in TACE or radiation in radioembolization remains unknown and could lead to a substantially different immune response. Our group is currently conducting experiments to further understand the impact of adding a pharmacological agent to TAE.

In conclusion, our results illustrate that transcatheter hepatic arterial bland embolization affects the tumor microenvironment by increasing infiltration of Th17 cells and expression of their signature cytokine IL-17. However, it did not have a significant effect upon migration of CD8 T cells or Tregs. In a simulated post-embolization environment, exogenous addition of IL-17 significantly reduced McA-RH7777 cell migration.

Funding This research was supported by BTG and SIO Immuno-Oncology-Interventional Oncology grant program, Biocompatibles UK Ltd (BTG), Surrey, UK, Grant# BTG-SP-08.004-F01, Sister Institution Network Fund (SINF) Grant# SINF-600801-80-115693-21, Department of Defense W81XWH-16-1-0100, and The University of Texas MD Anderson Cancer Center, and Center for Inflammation and Cancer Support Grant. The funders had no role in study design, data collection, analysis, interpretation of the data, decision to submit results, the decision to publish, or preparation of the manuscript.

Compliance with Ethical Standard

Conflict of interest All authors declare that they have no conflict of interest.

Ethical Approval All applicable international, national, and/or institutional guidelines for the care and use of animals were followed. All procedures performed in studies involving animals were in accordance with the ethical standards of the institution at which the studies were conducted. This article does not contain any studies with human participants performed by any of the authors.

References

1. Bruix J, Sherman M. Management of hepatocellular carcinoma: an update. Hepatology. 2011;53(3):1020–2. https://doi.org/10.1002/hep.24199.
2. EASL-EORTC clinical practice guidelines. management of hepatocellular carcinoma. J Hepatol. 2012;56(4):908–43. https://doi.org/10.1016/j.jhep.2011.12.001.
3. Brown KT, Do RK, Gonen M, Covey AM, Getrajdman GI, Sofocleous CT, et al. Randomized trial of hepatic artery embolization for hepatocellular carcinoma using doxorubicin-eluting microspheres compared with embolization with microspheres alone. J Clin Oncol. 2016;34(17):2046–53. https://doi.org/10.1200/jco.2015.64.0821.
4. Forner A, Llovet JM, Bruix J. Hepatocellular carcinoma. Lancet. 2012;379(9822):1245–55. https://doi.org/10.1016/s0140-6736(11)61347-0.
5. Garg AD, Galluzzi L, Apetoh L, Baert T, Birge RB, Bravo-San Pedro JM, et al. Molecular and translational classifications of DAMPs in immunogenic cell death. Front Immunol. 2015;6:588. https://doi.org/10.3389/fimmu.2015.00588.
6. Ayaru L, Pereira SP, Alisa A, Pathan AA, Williams R, Davidson B, et al. Unmasking of alpha-fetoprotein-specific CD4(+) T cell responses in hepatocellular carcinoma patients undergoing embolization. J Immunol. 2007;178(3):1914–22.
7. Liao J, Xiao J, Zhou Y, Liu Z, Wang C. Effect of transcatheter arterial chemoembolization on cellular immune function and regulatory T cells in patients with hepatocellular carcinoma. Mol Med Rep. 2015;12(4):6065–71. https://doi.org/10.3892/mmr.2015.4171.
8. Duan XH, Li TF, Zhou GF, Han XW, Zheng CS, Chen PF, et al. Transcatheter arterial embolization combined with radiofrequency ablation activates CD8(+) T-cell infiltration surrounding residual tumors in the rabbit VX2 liver tumors. Onco Targets Ther. 2016;9:2835–44. https://doi.org/10.2147/ott.S95973.
9. Anderson KG, Stromnes IM, Greenberg PD. Obstacles posed by the tumor microenvironment to T cell activity: a case for

synergistic therapies. Cancer Cell. 2017;31(3):311–25. https://doi.org/10.1016/j.ccell.2017.02.008.
10. Sharpe AH, Freeman GJ. The B7–CD28 superfamily. Nat Rev Immunol. 2002;2(2):116–26. https://doi.org/10.1038/nri727.
11. Wei SC, Duffy CR, Allison JP. Fundamental mechanisms of immune checkpoint blockade therapy. Cancer Discov. 2018;8(9):1069–86. https://doi.org/10.1158/2159-8290.Cd-18-0367.
12. Nishida N, Kudo M. Role of immune checkpoint blockade in the treatment for human hepatocellular carcinoma. Dig Dis. 2017;35(6):618–22. https://doi.org/10.1159/000480258.
13. Tang J, Shalabi A, Hubbard-Lucey VM. Comprehensive analysis of the clinical immuno-oncology landscape. Ann Oncol. 2017;29(1):84–91. https://doi.org/10.1093/annonc/mdx755.
14. Manieri NA, Chiang EY, Grogan JL. TIGIT: A key inhibitor of the cancer immunity cycle. Trends Immunol. 2017;38(1):20–8. https://doi.org/10.1016/j.it.2016.10.002.
15. Sharma P, Hu-Lieskovan S, Wargo JA, Ribas A. Primary, adaptive, and acquired resistance to cancer immunotherapy. Cell. 2017;168(4):707–23. https://doi.org/10.1016/j.cell.2017.01.017.
16. Zhang H, Song Y, Yang H, Liu Z, Gao L, Liang X, et al. Tumor cell-intrinsic Tim-3 promotes liver cancer via NF-kappaB/IL-6/STAT3 axis. Oncogene. 2018;37(18):2456–68. https://doi.org/10.1038/s41388-018-0140-4.
17. Li Z, Li N, Li F, Zhou Z, Sang J, Chen Y, et al. Immune checkpoint proteins PD-1 and TIM-3 are both highly expressed in liver tissues and correlate with their gene polymorphisms in patients with HBV-related hepatocellular carcinoma. Medicine (Baltimore). 2016;95(52):e5749. https://doi.org/10.1097/md.0000000000005749.
18. Anderson AC, Joller N, Kuchroo VK. Lag-3, Tim-3, and TIGIT: co-inhibitory receptors with specialized functions in immune regulation. Immunity. 2016;44(5):989–1004. https://doi.org/10.1016/j.immuni.2016.05.001.
19. Guo Y, Klein R, Omary RA, Yang GY, Larson AC. Highly malignant intra-hepatic metastatic hepatocellular carcinoma in rats. Am J Transl Res. 2010;3(1):114–20.
20. Takaki H, Imai N, Thomas CT, Yamakado K, Yarmohammadi H, Ziv E, et al. Changes in peripheral blood T-cell balance after percutaneous tumor ablation. Minim Invasive Ther Allied Technol. 2017;26(6):331–7. https://doi.org/10.1080/13645706.2017.1310737.
21. Munoz NM, Minhaj AA, Maldonado KL, Kingsley CV, Cortes AC, Taghavi H, et al. Comparison of dynamic contrast-enhanced magnetic resonance imaging and contrast-enhanced ultrasound for evaluation of the effects of sorafenib in a rat model of hepatocellular carcinoma. Magn Reson Imaging. 2019;57:156–64. https://doi.org/10.1016/j.mri.2018.11.012.
22. Nishiofuku H, Cortes AC, Ensor JE, Minhaj AA, Polak U, Lopez MS, et al. Factors impacting technical success rate of image-guided intra-arterial therapy in rat orthotopic liver tumor model. Am J Transl Res. 2019;11(6):3761–70.
23. Gaba RC, Emmadi R, Parvinian A, Casadaban LC. Correlation of doxorubicin delivery and tumor necrosis after drug-eluting bead transarterial chemoembolization of rabbit VX2 liver tumors. Radiology. 2016;280(3):752–61. https://doi.org/10.1148/radiol.2016152099.
24. Hendry S, Salgado R, Gevaert T, Russell PA, John T, Thapa B, et al. assessing tumor-infiltrating lymphocytes in solid tumors: a practical review for pathologists and proposal for a standardized method from the international immunooncology biomarkers working group: part 1: assessing the host immune response, TILs in invasive breast carcinoma and ductal carcinoma in situ, metastatic tumor deposits and areas for further research. Adv Anat Pathol. 2017;24(5):235–51. https://doi.org/10.1097/pap.0000000000000162.
25. Rhee TK, Larson AC, Prasad PV, Santos E, Sato KT, Salem R, et al. Feasibility of blood oxygenation level-dependent MR imaging to monitor hepatic transcatheter arterial embolization in rabbits. J Vasc Interv Radiol. 2005;16(11):1523–8. https://doi.org/10.1097/01.Rvi.0000182179.87340.D7.
26. Ma W, Jia J, Wang S, Bai W, Yi J, Bai M, et al. The prognostic value of 18F-FDG PET/CT for hepatocellular carcinoma treated with transarterial chemoembolization (TACE). Theranostics. 2014;4(7):736–44. https://doi.org/10.7150/thno.8725.
27. Kitamura K, Hatano E, Higashi T, Narita M, Seo S, Nakamoto Y, et al. Proliferative activity in hepatocellular carcinoma is closely correlated with glucose metabolism but not angiogenesis. J Hepatol. 2011;55(4):846–57. https://doi.org/10.1016/j.jhep.2011.01.038.
28. Liang CC, Park AY, Guan JL. In vitro scratch assay: a convenient and inexpensive method for analysis of cell migration in vitro. Nat Protoc. 2007;2(2):329–33. https://doi.org/10.1038/nprot.2007.30.
29. Schneider CA, Rasband WS, Eliceiri KW. NIH Image to ImageJ: 25 years of image analysis. Nat Methods. 2012;9(7):671–5.
30. Crowley LC, Christensen ME, Waterhouse NJ. Measuring Survival of Adherent Cells with the Colony-Forming Assay. Cold Spring Harb Protoc. 2016;2016(8). doi:10.1101/pdb.prot087171.
31. Franken NAP, Rodermond HM, Stap J, Haveman J, van Bree C. Clonogenic assay of cells in vitro. Nat Protoc. 2006;1(5):2315–9. https://doi.org/10.1038/nprot.2006.339.
32. Arifin WN, Zahiruddin WM. Sample Size Calculation in Animal Studies Using Resource Equation Approach. Malays J Med Sci. 2017;24(5):101–5. https://doi.org/10.21315/mjms2017.24.5.11.
33. Rohr-Udilova N, Klinglmuller F, Schulte-Hermann R, Stift J, Herac M, Salzmann M, et al. Deviations of the immune cell landscape between healthy liver and hepatocellular carcinoma. Sci Rep. 2018;8(1):6220. https://doi.org/10.1038/s41598-018-24437-5.
34. Liao Y, Wang B, Huang ZL, Shi M, Yu XJ, Zheng L, et al. Increased circulating Th17 cells after transarterial chemoembolization correlate with improved survival in stage III hepatocellular carcinoma: a prospective study. PLoS ONE. 2013;8(4):e60444. https://doi.org/10.1371/journal.pone.0060444.
35. Kim MJ, Jang JW, Oh BS, Kwon JH, Chung KW, Jung HS, et al. Change in inflammatory cytokine profiles after transarterial chemotherapy in patients with hepatocellular carcinoma. Cytokine. 2013;64(2):516–22. https://doi.org/10.1016/j.cyto.2013.07.021.
36. Zhou Y, Xu X, Ding J, Jing X, Wang F, Wang Y, et al. Dynamic changes of T-cell subsets and their relation with tumor recurrence after microwave ablation in patients with hepatocellular carcinoma. J Cancer Res Ther. 2018;14(1):40–5. https://doi.org/10.4103/jcrt.JCRT_775_17.
37. Qian X, Chen H, Wu X, Hu L, Huang Q, Jin Y. Interleukin-17 acts as double-edged sword in anti-tumor immunity and tumorigenesis. Cytokine. 2017;89:34–44. https://doi.org/10.1016/j.cyto.2015.09.011.
38. Asadzadeh Z, Mohammadi H, Safarzadeh E, Hemmatzadeh M, Mahdian-Shakib A, Jadidi-Niaragh F, et al. The paradox of Th17 cell functions in tumor immunity. Cell Immunol. 2017;322:15–25. https://doi.org/10.1016/j.cellimm.2017.10.015.
39. Benchetrit F, Ciree A, Vives V, Warnier G, Gey A, Sautes-Fridman C, et al. Interleukin-17 inhibits tumor cell growth by means of a T-cell-dependent mechanism. Blood. 2002;99(6):2114–211.
40. Wang L, Yi T, Kortylewski M, Pardoll DM, Zeng D, Yu H. IL-17 can promote tumor growth through an IL-6-Stat3 signaling pathway. J Exp Med. 2009;206(7):1457–64. https://doi.org/10.1084/jem.20090207.

41. Wu L, Chen X, Zhao J, Martin B, Zepp JA, Ko JS, et al. A novel IL-17 signaling pathway controlling keratinocyte proliferation and tumorigenesis via the TRAF4-ERK5 axis. J Exp Med. 2015;212(10):1571–87. https://doi.org/10.1084/jem.20150204.
42. Erinjeri JP, Thomas CT, Samoilia A, Fleisher M, Gonen M, Sofocleous CT, et al. Image-guided thermal ablation of tumors increases the plasma level of interleukin-6 and interleukin-10. J Vasc Interv Radiol. 2013;24(8):1105–12. https://doi.org/10.1016/j.jvir.2013.02.015.
43. Rozenblum N, Zeira E, Bulvik B, Gourevitch S, Yotvat H, Galun E, et al. Radiofrequency ablation: inflammatory changes in the periablative zone can induce global organ effects, including liver regeneration. Radiology. 2015;276(2):416–25. https://doi.org/10.1148/radiol.15141918.
44. Gu FM, Li QL, Gao Q, Jiang JH, Zhu K, Huang XY, et al. IL-17 induces AKT-dependent IL-6/JAK2/STAT3 activation and tumor progression in hepatocellular carcinoma. Mol Cancer. 2011;10:150. https://doi.org/10.1186/1476-4598-10-150.
45. Liao R, Sun J, Wu H, Yi Y, Wang JX, He HW, et al. High expression of IL-17 and IL-17RE associate with poor prognosis of hepatocellular carcinoma. J Exp Clin Cancer Res. 2013;32:3. https://doi.org/10.1186/1756-9966-32-3.
46. Yarchoan M, Xing D, Luan L, Xu H, Sharma RB, Popovic A, et al. Characterization of the immune microenvironment in hepatocellular carcinoma. Clin Cancer Res. 2017;23(23):7333–9. https://doi.org/10.1158/1078-0432.Ccr-17-0950.
47. Zhang Z, Yu X, Wang Z, Wu P, Huang J. Anthracyclines potentiate anti-tumor immunity: A new opportunity for chemoimmunotherapy. Cancer Lett. 2015;369(2):331–5. https://doi.org/10.1016/j.canlet.2015.10.002.